Unsteady Flow Organization of a Shock Wave/Turbulent Boundary Layer Interaction

R.A. HUMBLE,[1] F. SCARANO, and B.W. van OUDHEUSDEN

Faculty of Aerospace Engineering, Delft University of Technology

Kluyverweg 1, 2629 HS, Delft, The Netherlands, [1]*r.a.humble@tudelft.nl*

Abstract. The interaction between an incident shock wave and a turbulent boundary layer is investigated using Particle Image Velocity and Proper Orthogonal Decomposition in order to make statements regarding its unsteady flow organization. The interaction instantaneously exhibits a two-layer structure; namely, a high-velocity outer layer, and a low-velocity inner layer. Vortical structures are prevalent at their interface, which appear to play a role in the interaction between the two layers. Low-order eigenmodes show an energetic association between velocity fluctuations within the separated flow region and those along the reflected shock wave. The first eigenmode leads to a simple description of the flow unsteadiness: a less-full incoming boundary layer corresponds with a larger separation bubble, which in turn, corresponds with the reflected shock wave moving away from the wall and vice-versa.

Key words: shock wave, boundary layer, turbulence, POD.

1. Introduction

Shock wave/turbulent boundary layer interactions (SWTBLIs) have been the subject of high-speed fluid dynamics research for decades, but there still remain many open questions regarding even the most basic physical mechanisms. Among the interests of current researchers in recent years, has been the unsteady flow physics of such interactions. This has been largely due to the deficiencies of some of the most promising turbulence closure models [1], which generally remain hampered by the difficulties of modelling unsteady compressible flows, as well as the engineering implications associated with flowfield unsteadiness, such as premature structural fatigue.

An increasing body of experimental evidence has shown that SWTBLIs are unsteady flow phenomena, with a high-frequency small-scale motion, superimposed on a low-frequency large-scale motion (relative to U_∞/δ), of the shock system and separated flow region [2]. Whilst the small-scale motion has been attributed to the response to the convection of turbulent structures [3], identifying the cause(s) of the large-scale motion has proven to be more problematic. Several researchers have attempted to correlate the low-frequency shock wave motion with the upstream flow conditions [4], the internal dynamics of the separated flow region itself [5], as well as the proposal of large-scale unsteadiness due to an acoustic resonance mechanism [6]. Yet a complete theory explaining the underlying dynamics has not yet been formulated.

Much attention has therefore been devoted to the development of low-order, or simplified representations of more complicated fluid dynamical systems. This is often done with the intent of giving a relatively general description of the overall dynamics, with the belief that the dominant flow physics will be retained. This has led to the development of statistical techniques such as the Proper Orthogonal Decomposition (POD) in particular [7]. This technique has been introduced into fluid mechanics as a tool to highlight coherent motions within turbulent flows. This can then often be used to facilitate the development of a low-order description of the overall dynamics.

The present paper investigates an incident SWTBLI with the objectives of shedding some light on its dynamical features and formulating a conceptual picture of its organized global dynamics. Whole-field instantaneous velocity fields are obtained by means of Particle Image Velocimetry (PIV). Further discussion is given on the determined vortical structure pattern. The velocity data are then analyzed by POD to investigate the underlying unsteady flow organization, as revealed by the global eigenmodes. A simple physical model is proposed based upon the first eigenmode. The statistical description of the flow has been reported in a previous work [8].

2. Apparatus and Experimental Technique

2.1. FLOW FACILITY AND PIV TECHNIQUE

Experiments were performed in the blow-down transonic-supersonic wind tunnel (TST-27) at Delft University of Technology. Test section dimensions are 300mm×270mm. The boundary layer on the wind tunnel top wall was used. Upon entering the measurement domain, its thickness was δ_{99}=20mm [8]. A shock generator was placed in the middle of the test section to generate the incident shock wave. The generator consisted of a 100mm long single-sided wedge giving a deflection angle of 8°. It was mounted on one side of the wind tunnel and spanned 96% of the test section. A multi-planar assessment of the interaction [8] confirmed that the mean flowfield properties did not change appreciably within the spanwise region considered ($-2.5 \le z/\delta \le 2.5$). The wind tunnel was operated at a stagnation pressure of 276kPa and stagnation temperature of 286K. The nominal freestream Mach number was M_∞=2.1 (U_∞=518m/s) and $Re_\theta=4.92\times10^4$ based upon the undisturbed boundary layer. A schematic representation of the experimental configuration is shown in Figure 1.

Two-component PIV is employed in the present study. A 2-D rake seeded the flow in the settling chamber with titanium dioxide (TiO_2) particles, with a median diameter of 400nm and bulk density of 200kg/m^3. Flow illumination was provided by a Big Sky CFR PIV-200 Nd:Yag laser with 200mJ pulsed energy and a 7ns pulse duration at wavelength 532nm. Laser light access was provided by a probe inserted into the flow downstream of the model. The laser pulse separation was 2μs, resulting in a particle displacement of 1mm in the freestream flow. The light sheet was approximately 1.5mm thick.

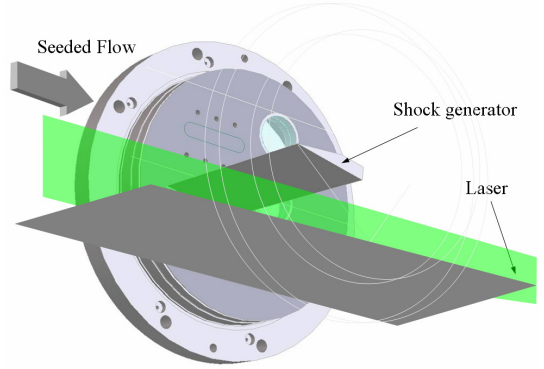

Figure 1. Experimental setup

Images were recorded at 10Hz by a PCO Sensicam QE, a 12-bit CCD camera with a 1376×1040 pixel-sized sensor. Only 416 pixel rows were used given the large aspect ratio of the investigated flow region. The camera was equipped with a Nikon 60mm focal objective with a numerical aperture $f_{\#}$=8, in combination with a narrow-band-pass 532nm filter. The flow was imaged over a field-of-view of 129mm×40mm, resulting in a digital resolution of 11pixels/mm. A dataset of 500 image pairs was acquired. The recorded images were interrogated using the two-dimensional cross-correlation algorithm WIDIM [9]. The images were interrogated using rectangular windows of size 21×17 pixels and an overlap factor of 75%, resulting in a window size of 1.9×1.6mm^2.

2.2. DATA REDUCTION

The POD is used to decompose the time variation of the flowfield into a limited number of modes that capture the most dynamically significant features. The data represent fluctuating velocity obtained from the PIV study. The snapshot method, as first proposed by Sirovich [10], is implemented in the present study. Consider a system where data measurements are taken at M time instants t_n. The POD extracts k time-independent orthonormal basis functions, empirical eigenfunctions, or eigenmodes, $\psi_k(x, y)$, and time-dependent orthonormal amplitude coefficients, $a_k(t_n)$, such that

$$u(x,y,t_n) = \bar{u}(x,y) + \sum_{k=1}^{M} a_k(t_n)\psi_k(x,y) \qquad n = 1,\ldots,M \tag{1}$$

is optimal, in the sense that ψ maximizes the normalized averaged projection of u onto ψ [7]. Here, $\bar{u}(x, y)$ is the mean velocity field. The total energy of the flow is defined as the sum of the eigenvalues λ_k, each eigenmode being assigned an energy percentage

$$E_k = \lambda_k \Big/ \sum_{i=1}^{M} \lambda_i \tag{2}$$

In compressible flows, the best choice of norm is not obvious: many of the (interrelated) variables, including thermodynamic quantities, can be important [11]. In the present paper, the mean square fluctuating value of velocity is used.

3. Results and Discussion

3.1. INSTANTANEOUS FLOW ORGANIZATION

Figure 2 illustrates uncorrelated fields of instantaneous streamwise velocity, with velocity vectors (under-sampled showing 1 in 22 in the streamwise direction). Figures 2a–c show that fluid close to the wall is redirected upstream, leading to the formation of a separated flow region. This configuration forces outer fluid to move away from the wall. The separation bubble length varies in the range between 0–2δ (compare for instance Figures 2c and 2d), with the velocity in the reversed-flow region often attaining a value 10% of U_∞. However, according to the average velocity field, the boundary layer remains attached, indicating that reversed-flow occurs only instantaneously [8].

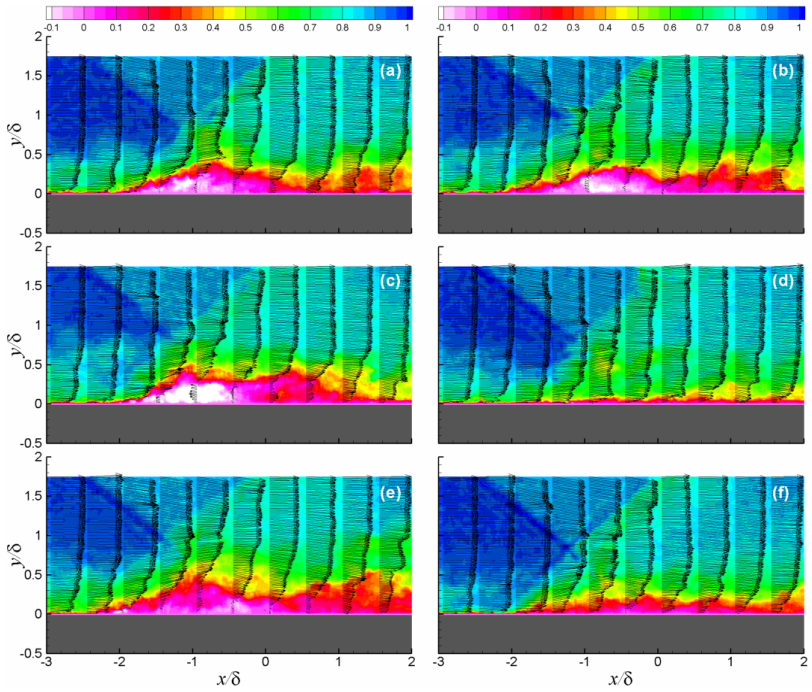

Figure 2. Uncorrelated instantaneous streamwise velocity distributions u/U_∞. Velocity vectors show 1 in 22 in the streamwise direction.

Figures 2a–c, and 2e show irregularly shaped layers of relatively uniform streamwise velocity, readily observed in the velocity vectors within the redeveloping boundary layer. The term *layer* is used here to emphasize that whilst they are defined instantaneously, they typically extend across the measurement domain. The interaction typically contains a high-velocity outer layer (typically u/U_∞>0.5), and a low-velocity inner layer (typically u/U_∞<0.5). The outer layer comprises most of the incoming boundary layer. It retains most of its streamwise velocity throughout the interaction. In contrast, a noticeable reduction in streamwise velocity occurs within the inner layer. This layer contains values of the same order as found within the near-wall region of the incoming boundary layer. It grows rapidly as it enters the first part of the interaction, often reaching its maximum thickness when it intersects with the incident shock wave.

The two layers are typically separated by a thin region of relatively high shear. Figures 2b and 2c show outer fluid penetrating deep into the boundary layer. The interface therefore has an irregular and intermittent nature, which is a particularly dominant feature of the redeveloping boundary layer. Figures 2b, 2c, and 2e show the interface has a downstream-sloping pattern. Furthermore, the interface appears to be more distinct in the first part of the interaction region, than farther downstream. Spatio-temporal studies of incident SWTBLI's have determined that frequencies tend to decrease along the separated flow region [12], noting that in subsonic recirculating flows, such frequency evolutions are associated with large-scale structures convected in a mixing layer, which develops downstream of flow detachment. It therefore appears possible that vortical structures grow and develop within the separated shear layer. Another feature, shown in Figures 2a–c, is that while the reattachment process takes place within a relatively short streamwise extent, the overall velocity deficit within the inner layer persists much farther downstream.

3.2. IDENTIFICATION OF VORTICAL STRUCTURES

Following the method proposed by Hunt *et al.* [13], vortical structures are identified as any contiguous region of flow where the second invariant Q of the velocity gradient tensor is greater than zero. In the present paper, it is assumed that the criterion $Q>0$ is valid in compressible flow, since the divergence of velocity was found to be small, and because results were obtained that were very similar to the use of other (incompressible) criterion, such as the λ_2 criterion [14]. Note that the following determined patterns are only a section of the complete three-dimensional structure from the x–y plane, and therefore represent only a footprint of the spanwise vortical structure of the interaction.

Figure 3 shows contours of $Q>0$, with a non-zero threshold to distinguish from measurement noise. Under-sampled velocity vectors, displaying 1 in 5 in the streamwise direction are shown, with a convective velocity of $U_c=0.7U_\infty$. (Note that each figure part corresponds to the preceding figure parts of Figure 2.) The results reveal distinct regions of $Q>0$, which are interpreted to be sections through vortical structures. These structures exhibit a variety of size and spatial organization, without any trace of the wall-bounded shear region. Structures can also be distinguished within the undisturbed boundary layer. Figures 3b, 3c, and 3e show vortical structures approaching the interaction, where they are lifted away from the wall, upwards into the shear layer in the detachment region. They appear to turn around the bubble, often impinging on the wall in the reattachment region. A similar observation can also be made in Figure 3f when the boundary layer remains attached. Very few vortical structures can be observed within the separated flow region, despite large velocity fluctuations being present [8]. Rather, vortical structures are typically found along the interface between the two layers. This can be understood when it is realized that this interface is a region of large $\partial u/\partial y$—it is therefore a source of spanwise vorticity. As a matter of fact, the two layers are delineated by an interface which contains discrete, concentrated regions of spanwise vorticity, which generally correspond to the locations of vortical structures. The inner layer can, therefore, be viewed as acting like a streamlined obstacle.

Interestingly, vortical structures appear to propagate mainly in the region where the incident shock wave intersects (and terminates) at the sonic line. This confirms a direct numerical simulation (DNS) of an incident SWTBLI [6], where it was found that the oscillatory motion of the incident shock wave occurs mainly at its tip. It is important to emphasize, that these discrete vortical structures do not necessarily represent disconnected regions of vorticity; more likely, they are connected out of the plane of the laser sheet forming a highly complicated flow pattern.

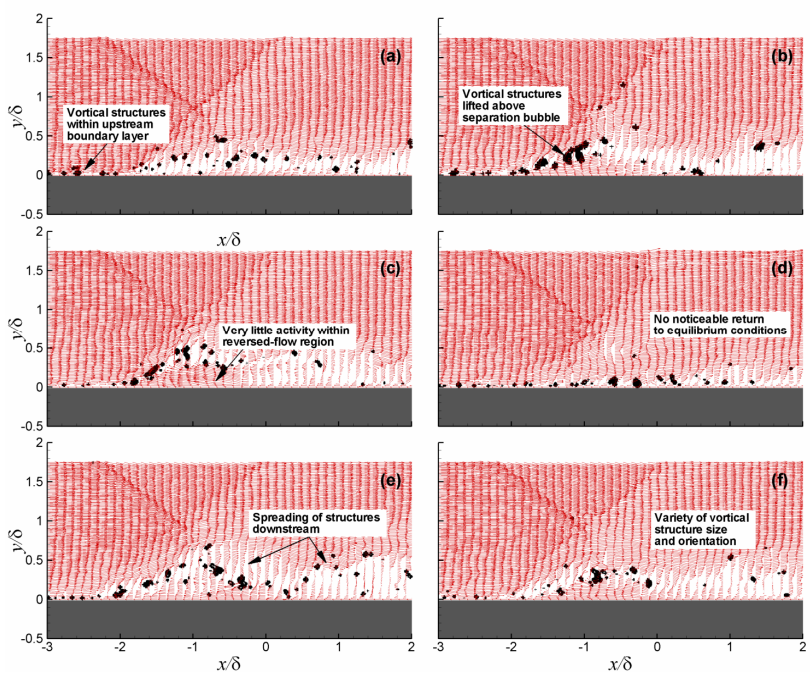

Figure 3. Vortical structures within the interaction using the Q criterion. Contours of Q>0, along with convective velocity vectors U_c=0.7U_∞ showing 1 in 5 in the streamwise direction.

Convective velocity vectors show that fluid is drawn in and ingested in between the two layers. The reattachment of the separated shear layer depends critically upon the ability of the fluid along the dividing streamline overcoming the pressure gradient at reattachment. This ability is a function of the momentum available, which can be increased by entraining outer fluid. It appears that the vortical structures play a role in this process, by supplying fluid to the inner layer. This is in fact, not dissimilar to the scenario that has been described in low-speed separated flows [15], which discuss how movies of laser-illuminated smoke and turbulence energy results reveal how large-scale eddy structures supply the near wall separated flow. Farther downstream, vortical structures become more broadly distributed normal to the wall. (Figure 3e is a good example.) Wall-normal turbulence intensity profiles have been shown to spread more broadly over the vertical height of the interaction than the streamwise intensity [8]. This indicates that, in contrast to what occurs within the undisturbed boundary layer, a significant vertical mixing takes place away from the wall. Here, it is anticipated that the shear layer instability yields a high kinetic energy transfer from the mean flow to the vortical structures, and they are expected to play an important role in extracting energy from the mean shear and transferring it to subsequently smaller structures.

3.3. POD ANALYSIS

Having conceptually outlined some of the physical mechanisms, we now construct a simplified description of the dynamical behaviour using POD. Physically, each eigenmode can be considered as capturing an independent predominant dynamical characteristic of the flow, which may not be revealed by the instantaneous flow realizations. Although the interpretation of eigenmodes as representing physical flow phenomena has long been a source of debate, one general consensus is that it relies chiefly upon the energy convergence. As a motivating prelude, the eigenmode and cumulative eigenmode energy distributions are shown in Figures 4a and 4b respectively.

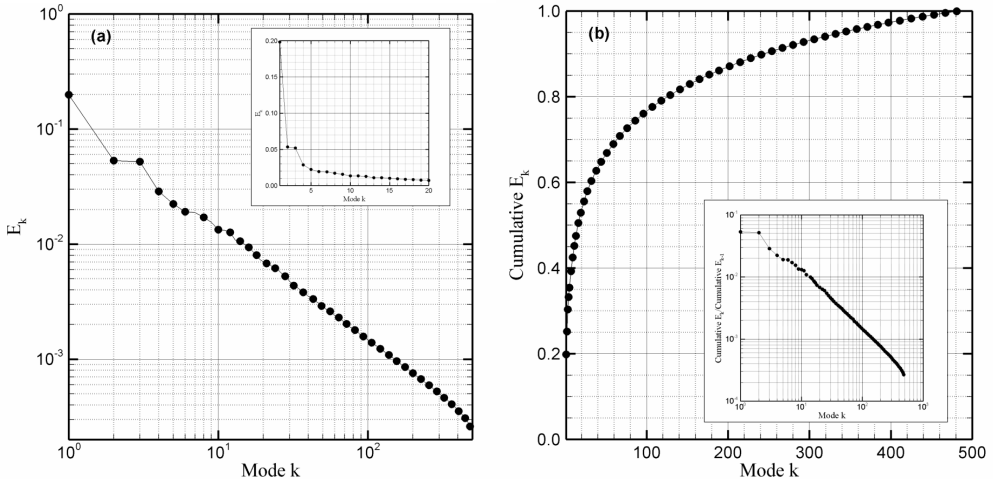

Figure 4. (a): Eigenmode energy distribution (inset: first 20 modes), (b): Cumulative energy distribution (inset: ratio of cumulative sums).

The present eigenmode energy distributions generally reflect a poor energy convergence when compared with other POD analyses of turbulent wall-bounded flows (e.g. Ref. [16]), where a larger amount of energy is typically captured by a relatively smaller number of eigenmodes (60% in first mode [16]). This discrepancy is ascribed to the comparably high Reynolds number of the present experiment, which leads to energy being distributed among a larger number of modes. Furthermore, the presence of random noise and occasional poor data quality, naturally present in experiments, also lead to energy being distributed among a larger number of modes. In order to visualize the dynamics associated with the present eigenmodes, we first create a 1–D Euclidean phase space ϕ using the temporal coefficients from the analysis. One can arbitrarily choose a finite number K of the most energetic modes, to form a subspace spanned by the first K eigenmodes. Similarly, subspaces can be formulated based upon a single eigenmode, by first ordering the temporal coefficients of all M observations, such that $\phi_n^k=\{a_k(t_n)\leq a_k(t_{n+1})\leq\ldots\leq a_k(t_M)\}$. An eigenmode then yields M subspaces, the nth subspace of the kth eigenmode $u_n^k(x, y)$ given by

$$u_n^k(x,y) = a_k(t_n)\psi_k(x,y), \quad n = 1,...,M \tag{3}$$

These subspaces provide a convenient method to analyze the dynamical behaviour given by the *k*th eigenmode. For notational convenience, we first define ϕ as

$$\phi_n^k = \begin{cases} 0 & \text{when} \quad a_k = \left(a_k\right)_{\min}; \quad n = 1 \\ \dfrac{1}{2} & \text{when} \quad a_k = \left(a_k\right)_{\max}; \quad n = M \end{cases} \tag{4}$$

Eigenmodes 1, 2, and 4 depict the streamwise and vertical velocity components in Figure 5 (left and right respectively). Figures 5a and 5c show a quasi-streamwise velocity pattern, with relatively large streamwise velocity fluctuations within the incoming boundary layer and separated flow region. Figures 5b and 5d show a phasewise alternation along the reflected shock wave. This indicates a cyclic motion, and its association with the incoming boundary layer and separated flow region is intriguing. Note the lack of velocity fluctuations along the incident shock wave, indicating that it is a steady feature.

Higher-order eigenmodes show a more intricate structure. Subspace bifurcations take place within the separated flow and reflected shock wave regions. The term *bifurcation* refers to the qualitative changes. Such bifurcations are associated with the higher-order harmonics required to properly represent the high-dimensional phase space of the data. Coherent flow features bifurcate to become smaller-scale motions, and it is interesting to observe that this occurs mainly within the redeveloping boundary layer. One may speculate that they are associated with the propagation of perturbations within the redeveloping boundary layer, as tentatively suggested by the instantaneous realizations. The magnitude of the vertical velocity fluctuations along the reflected shock wave decreases with increasing mode number, indicating that its motion is energetically associated with the more dominant, low-order eigenmodes. It therefore appears that the association between the incoming boundary layer, separated flow region, and reflected shock wave unsteadiness energetically dominate the dynamics of this flow.

The first eigenmode represents the most dynamically significant aspect of the flow. If it is projected onto the mean flow and animated in ϕ, then the simple physical model described, is that a less-full incoming boundary layer corresponds with a larger separation bubble, which in turn, corresponds with the reflected shock wave moving away from the wall and vice-versa. Changes in the incoming boundary layer profile relate to changes in the size of the separation bubble because of its change in resistance to flow separation. At the same time, the size of the separation bubble influences the motion of the separated shear layer and reflected shock wave. This is consistent with other models that have been proposed [17]. Although it cannot describe the interaction's complete behaviour, it is substantiated by what often occurs in the instantaneous realizations. (Compare Figures 2d and 2f with 2c and 2e. The reader will note that a less-full boundary layer indeed corresponds with a larger separated flow region, and a reflected shock wave which appears farther from the wall.) It is therefore remarkable that the incident shock wave, compression ramp, and blunt fin interactions, whose overall flow structures are very different, share at least one common mechanism [18].

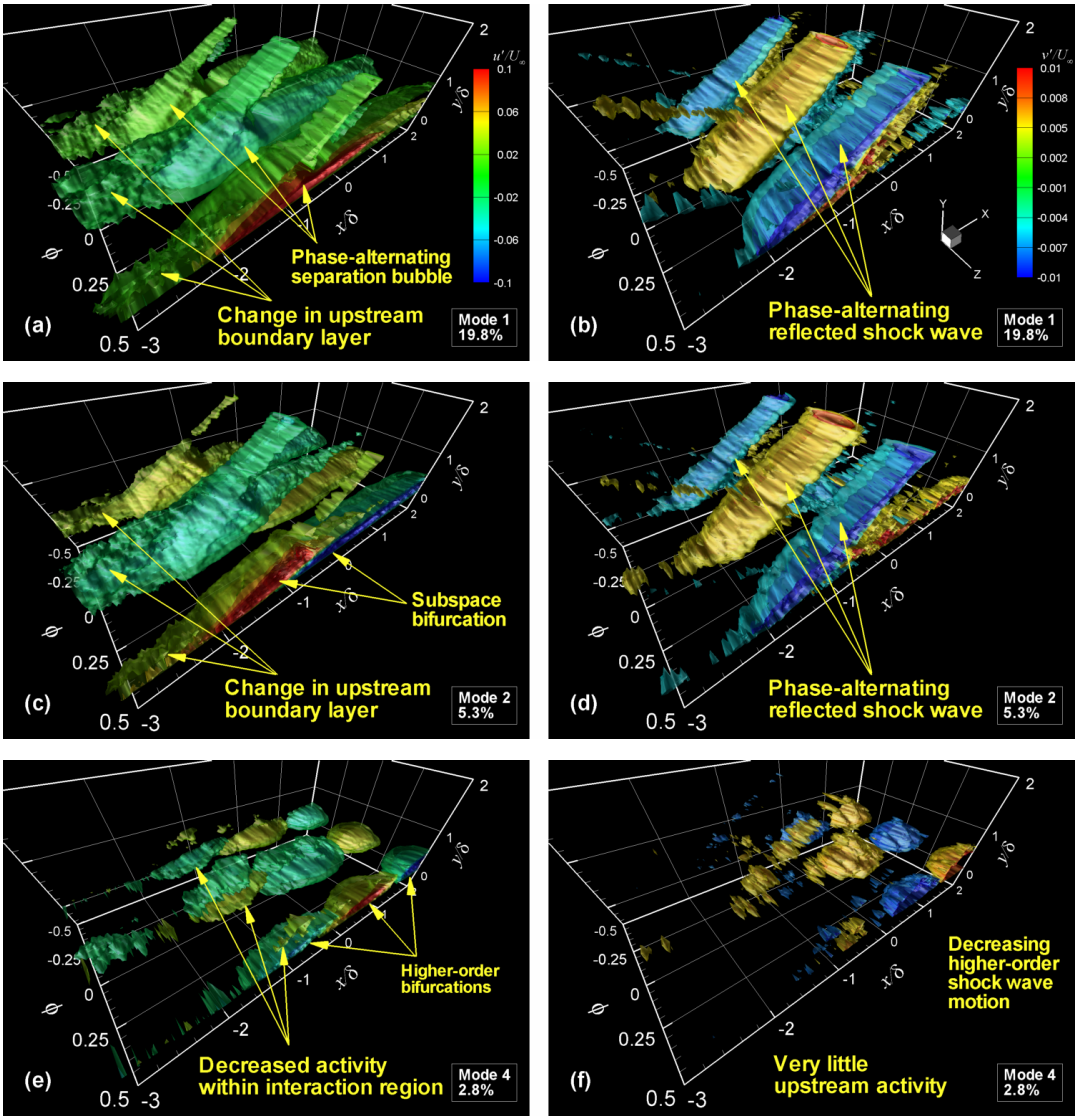

Figure 5. POD eigenmodes for u'/U_∞ (left) and v'/U_∞ (right). (Note: modes 2 and 4 show $2u'/U_\infty$)

4. Conclusions

The unsteady flow organization of an incident SWTBLI has been investigated using PIV and POD. Generally, the interaction instantaneously exhibits a two-layer structure; namely, a high-velocity outer layer, and a low-velocity inner layer. Vortical structures are prevalent at their interface, which appear to play a role in the interaction between the two layers. Low-order eigenmodes show an energetic association between streamwise velocity fluctuations within the separated flow region and vertical velocity fluctuations along the reflected shock wave. Higher-order eigenmodes show subspace bifurcations leading to coherent flow features that are energetically associated with smaller-scale motions. The first eigenmode represents a simple physical model: a less-full incoming boundary layer corresponds with a larger separation bubble, which in turn, corresponds with the reflected shock wave moving away from the wall and vice-versa.

Acknowledgements

This work is supported by the Dutch Technology Foundation STW under the VIDI—*Innovation Impulse* program, grant DLR.6198.

References

1. Knight, D.D., and Degrez, G., Shock wave boundary layer interactions in high speed flows. A critical survey of current numerical prediction capabilities, Advisory Rept. 319, AGARD **2** (1998) pp. 1.1—1.35.
2. Dolling, D.S., Fifty years of shock wave/boundary layer interaction research: what next?, *AIAA J.* **39** (2001) 1517—1531.
3. Erengil, M.E., and Dolling, D.S., Physical causes of separation shock unsteadiness in shock wave/turbulent boundary layer interactions, AIAA Paper 93-3134, (1993).
4. Andreopoulos, J., and Muck, K.C., Some new aspects of the shock-wave/boundary-layer interaction in compression flows, *J. Fluid Mech.* **180** (1987) 405—428.
5. Dolling, D.S., and Murphy, M.T., Unsteadiness of the separation shock wave structure in a supersonic compression ramp flowfield, *AIAA J.* **21** (1983) 1628—1634.
6. Pirozzoli, S., Grasso, F., Direct numerical simulation of impinging shock wave/turbulent boundary layer interaction at M=2.25, *Phys. Fluids* **18** 065113 (2006).
7. Holmes, P., Lumley, J.L., and Berkooz, G., Turbulence, coherent structures, dynamical systems and symmetry. Cambridge University Press, UK, (1996).
8. Humble, R.A., Scarano, F., and van Oudheusden, B.W., Experimental study of an incident shock wave/turbulent boundary layer interaction using PIV, 36th AIAA Fluid Dynamics Conference & Exhibit, San Fr., CA, (2006).
9. Scarano, F., Iterative image deformation methods in PIV, *Meas. Sci. and Tech.* **13** (2002) R1−R19.
10. Sirovich, L., Turbulence and the dynamics of coherent structures, *Q. Appl. Math.* XLV (1987) 561—590.
11. Rowley, C.W., Colonius, T., and Murray, R.M., Model reduction for compressible flows using POD and Galerkin projection, *Physica D* **189** (2004) 115—129.
12. Dupont, P., Haddad, C., and Debiève, J. F., Space and time organization in a shock-induced separated boundary layer, *J. Fluid Mech.* **559** (2006) 255—277.
13. Hunt, J.C.R., Wray, A.A., and Moin, P., Eddies, streams, and convergence zones in turbulent flows, *Center for Turbulence Research Report*, CTR-S88 (1988) 193—208.
14. Jeong, J., Hussain, F., Schoppa, W., and Kim, J., Coherent structures near the wall in a turbulent channel flow, *J. Fluid Mech.* **332** (1997) 185—214.
15. Simpson, R.L., Chew, Y.-T, and Shivaprasad, B.G., The structure of a separating turbulent boundary layer. Part 2. Higher-order turbulence results, *J. Fluid Mech.* **113** (1981) 53—73.
16. Aubry, N., Holmes, P., Lumley, J.P., and Stone, E., The dynamics of coherent structures in the wall region of the turbulent boundary layer, *J. Fluid Mech.* **192** (1988) 115—173.
17. Beresh, S.J., Clemens, N.T., and Dolling, D.S., Relationship between upstream turbulent boundary-layer velocity fluctuations and separation shock unsteadiness, *AIAA J.* **40** (2002) 2412—2422.
18. Ünalmis, Ö.H., and Dolling, D.S., Experimental study of causes of unsteadiness of shock-induced turbulent separation, *AIAA J.* **36** (1998) 371—378.